Environmental Science & Technology

pubs.acs.org/est

Article

Impact of Airborne Pathogen-Derived Extracellular Vesicles on Macrophages Revealed by Raman Spectroscopy and Multiomics

Published as part of the Environmental Science & Technology virtual special issue "The Exposome and Human Health".

Yifei Qin, Zheng Shi, Longji Zhu, Hongzhe Li, Wenjia Lu, Guozhu Ye, Qiansheng Huang,* and Li Cui*

Cite This: https://doi.org/10.1021/acs.est.3c04800

Read Online

ACCESS | Metrics & More | Article Recommendations | Supporting Information

ABSTRACT: Long-term exposure to the indoor environment may pose threats to human health due to the presence of pathogenic bacteria and their byproducts. Nanoscale extracellular vesicles (EVs) extensively secreted from pathogenic bacteria can traverse biological barriers and affect physio-pathological processes. However, the potential health impact of EVs from indoor dust and the underlying mechanisms remain largely unexplored. Here, Raman spectroscopy combined with multiomics (genomics and proteomics) was used to address these issues. Genomic analysis revealed that *Pseudomonas* was an efficient producer of EVs that harbored 68 types of virulence factor-encoding genes. Upon exposing macrophages to environmentally relevant doses of *Pseudomonas aeruginosa* PAO1-derived EVs, macrophage internalization was observed, and release of inflammatory factors was determined by RT-PCR. Subsequent Raman spectroscopy and unsupervised surprisal analysis of EV-affected macrophages distinguished metabolic alterations, particularly in proteins and lipids. Proteomic analysis further revealed differential expression of proteins in inflammatory and metabolism-related pathways, indicating that EV exposure induced macrophage metabolic reprogramming and inflammation. Collectively, our findings revealed that pathogen-derived EVs in the indoor environments can act as a new mediator for pathogens to exert adverse health effects. Our method of Raman integrated with multiomics offers a complementary approach for rapid and in-depth understanding of EVs' impact.

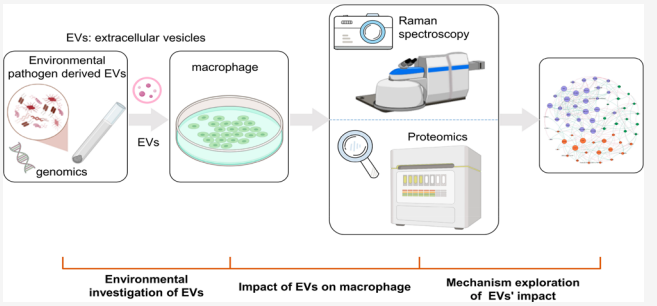

KEYWORDS: *extracellular vesicles, virulence factors, Raman spectroscopy, multiomics, urban health*

1. INTRODUCTION

As people spend increasing time on indoor activities, the indoor environment has become a critical factor affecting public health.[1] Indoor air is a complex mixture of various chemical and biological pollutants, many of which can accumulate on environmental surfaces and persist in the form of dust.[2] Potential pathogens, such as *Neisseria meningitidis*, *Mycobacterium tuberculosis*, *Escherichia coli*, and *Staphylococcus aureus* were found in indoor dust and can enter the human body through hand-to-mouth contact and breathing.[3]

Extracellular vesicles (EVs) have emerged as key players in the intercellular communication between bacteria and hosts. These lipid-bilayered membranous structures have a size range of 30−400 nm and are universally released by all domains of life.[4,5] EVs from pathogenic bacteria encompass regulatory mediators like nucleic acids, proteins, lipids, and carbohydrates.[6,7]

Growing evidence showed pathogens released EVs as "long-distance weapons" into host circulation and exerted profound influences on physiological and pathological processes.[8,9] EVs are also small enough, enabling them to traverse through human biological barriers, such as the blood−brain barrier to accelerate pathogenic infections.[10] EVs derived from *Pseudomonas aeruginosa* contain lipopolysaccharides (LPS) and other virulence factors (VFs) which can modulate the innate immune response and the local proinflammatory response of the host, and eventually led to chronic infection.[11] Furthermore, EVs from pathogenic *Neisseria gonorrheae*, *E. coli*, and *P. aeruginosa* have been shown to be able to destroy mitochondrial functions and induce immune responses in macrophages.[12] Additionally, fusobacterium nucleatum induced gastric cancer cell EVs secretion, thus triggering the activation of the microRNA-885-3p/EphB2 signaling pathway and subsequently resulting in enhanced proliferation, migration, and invasion ability of gastric cancer cells. These studies were primarily conducted under laboratory conditions. To our knowledge, there is only one study

Received: June 20, 2023
Revised: September 20, 2023
Accepted: September 21, 2023

reported that EVs from indoor dust in a dormitory building can promote the occurrence of lung cancer in mice.[13] Overall, we are still lacking a comprehensive understanding on which pathogenic species release EVs and how these EVs exert adverse effects on the host, impeding us from evaluating the potential health risks associated with environmental EVs. Perhaps rigorous investigation has been carried out on the functional attributes of EVs from a specific species; however, this species might only discharge a restricted amount of EVs in its natural environment. Hence, it is necessary to explore the source, specific contents, health risk, and molecular mechanisms of EVs in the field.

Recently, sequencing technology like transcriptomics and proteomics have emerged to reveal how cells respond to pathogenic EVs infection. However, focusing on a change in one specific component could not represent the whole picture of the host response. These sequencing technologies tend to target highly expressed genes and subtle metabolic changes, thus leading to an incomplete assessment of the overall response.[14] Raman spectroscopy is an optical scattering technique that enables the investigation of the vibrational motions of molecules, making it a good way to detect endogenous metabolites in a label-free manner.[15] Raman spectroscopy offers phenotypic and metabolic analysis by forming a detailed chemical "fingerprint" of all biomolecules in cells.[16] Raman spectra can identify various cellular metabolites,[17] including lipids, amino acids, nucleic acids, carbohydrates, cytochrome, etc. This technique can offer panoramic insights into comprehensive changes within the cell by incorporating information from transcriptomes, metabolomes, and proteomes. Moreover, spontaneous Raman spectroscopy acts like a snapshot camera, taking only a few seconds to acquire a complete cell spectrum and capture many types of molecular changes. While Raman spectroscopy can quickly reflect cells' overall phenotypic and metabolic states, it lacks a detailed description of specific molecular (like a particular gene or protein) characteristics. Therefore, combining Raman spectroscopy with sequencing technology may help us to better reveal the molecular change mechanism of the host.

In this work, we employed a multifaceted approach to investigate the characteristics and potential health risks of pathogenic EVs in an indoor environment. EVs were isolated from the dust of typical indoor fields, and their pathogenic source and contents were analyzed by metagenomic sequencing. Then, the pathogen-derived EVs with relatively high abundance in the indoor dust were applied to treat macrophages, and the global phenotypic and metabolic changes in macrophages were investigated via Raman spectroscopy with advanced data processing algorithms as well as proteomics. This study provided new insight into the health risk of EVs from the real environment.

2. MATERIALS AND METHODS

2.1. Sites and Sampling of Indoor Dust. Indoor dust was sampled from Xiamen, China (24°34′N, 118°04′E) with a vacuum cleaner during the summer of 2020 as we previously reported.[18] These sites are specific life fields, including kindergarten, restaurants, dormitories, and vehicles, all of which are closely related to human health. Dust was collected from furniture surfaces, including floors, shelves, and tables, as well as air conditioner filters. Due to difficulties in collecting dust from within vehicles, dust from the vacuum cleaner was used instead. At each sampling site, at least three indoor dust sites were collected and mixed to minimize the random errors. In order to maintain the in situ environment as much as possible, all the dust samples were stored at 4 °C and applied to EV extraction within 2 days after collection.

2.2. Bacteria Strains. *P. aeruginosa* PAO1 was isolated and identified by our lab. Bacteria were cultured at 37 °C in Lysogeny Broth Medium (Sinopharm Chemical Reagent Co, China).

2.3. Cell Line and Cell Culture. The THP-1 monocyte cell line used in this study was purchased from the Cell Bank of Type Culture Collection, Chinese Academy of Sciences (Shanghai, China). For more details on cell culture please refer to the Text S1.

2.4. Isolation of EVs from Dust and Bacterial Culture. Dust and bacterial EVs were isolated following a previous study with modifications.[13] Indoor dust was suspended in PBS with a solution ratio of 1:25 (weight:volume). To maintain the in situ environment, the mixed solution was incubated at 4 °C and shaken at 180 rpm for 12 h. The suspensions were filtered with 75 μm gauze to eliminate insoluble matters. The PAO1 bacteria were cultured in LB broth until the exponential growth stage at 37 °C and 180 rpm. The dust and bacterial suspensions were centrifuged at 8,000*g* for 20 min at 4 °C to remove bacteria and filtered sequentially through 0.45 and 0.22 μm PVDF filters (Millipore). The remaining particles were centrifugated again at 10,000*g* for 45 min at 4 °C and then ultracentrifugated at 120,000*g* for 90 min at 4 °C to finally pellet EVs. The pellet was redissolved with PBS using the above centrifugation condition to purify EVs, which were then stored at −80 °C for further experiments.

For the obtained environmental EVs, we performed DNA extraction and metagenomic sequencing. For a large number of consistent EVs from *P. aeruginosa*, we investigated the biological functions of EVs. Additionally, it is important to note that the EVs used in this study specifically refer to particles within the size range of tens to two hundred nanometers.

2.5. Characterization of EVs. Transmission electron microscopy (TEM) and nano flow cytometry (nano FCM) were applied to characterize the EVs. For TEM analysis, EVs in PBS were negatively stained with 1% uranium oxaloacetate and imaged with the Tecnai G2 Spirit transmission electron microscope (Hitachi, JPN) after settling on a copper mesh for 1 min. For nanoflow cytometry (N30, NanoFCM, Xiamen, China) analysis, EVs' size distribution and particle concentration are referenced with those of silica nanospheres ranging from 68 to 155 nm. Three measurement replicates were performed.

2.6. Calculation of Environmentally Relevant Doses of EVs in the Cell Experiment. Dust can enter the human body through respiratory exposure and hand−mouth contact, with children being the main group at risk. The U.S. Environmental Protection Agency (EPA) estimated that children aged 1−6 years ingest 100 mg/day.[19] By simulating the frequency of contacts of children aged 3 to 6, Ozkaynak et al. reported the average total soil/dust ingestion rate (IR) at 68 mg/day, where at the 95th percentage level, it can be as high as 224 mg/day.[20] Through our previous research and other evidence[13,18] indoor dust can contain up to 10^{11} particle EVs per gram. Considering the amount of indoor dust inhaled by humans daily, the amount of EVs in each person daily intake can be calculated as follow:

$$10^{11}\ \text{EVs/gram} \times 100\ \text{mg/day} = 10^{10}\ \text{EVs/day}$$

https://doi.org/10.1021/acs.est.3c04800
Environ. Sci. Technol. XXXX, XXX, XXX−XXX

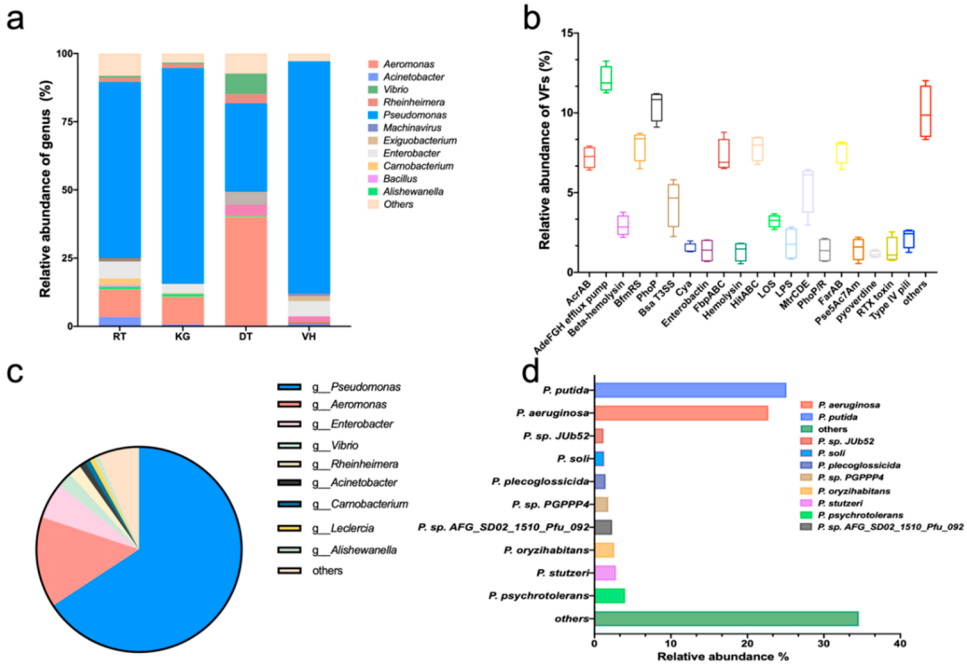

Figure 1. Source taxonomic profiles and distribution of VFs in indoor dust-derived EVs. (a) Dominant genera present in indoor dust-derived EVs (top 10 in each group). restaurant, RT; kindergarten, KG; dormitory, DT; and vehicle, VH. (b) Relative abundance of the top 20 VF types in indoor dust-derived EVs. (c) Proportion of EVs-associated VFs carried by different microbes in the indoor environment. (d) The relative abundance of EV-releasing strains of Pseudomonas in the indoor dust.

In this work, we measured the total protein content of EVs. The total protein quantity of each 2×10^{10} EVs is 10 μg. Thus, we selected EVs concentrations at 1, 5, and 10 μg proteins/mL (the corresponding EV number is 4×10^9, 2×10^{10}, 4×10^{10}) to expose macrophages. Meanwhile, the exposure dose is lower than in previous studies,[12,13] which also used *P. aeruginosa* EVs to expose cells. Therefore, the concentrations used in this experiment are suitable for mimicking the inhaled exposure dose of dust EVs for one person and show environmental relevance. However, as the difference between the in vitro cell model and in vivo model, the concentration cannot represent the doses a macrophage can encounter in the lung environment.

2.7. EVs Labeling and Tracking. EVs were resuspended in PBS and stained with Dio green Fluorescent dye (Beyotime, Beijing, China). After 30 min of incubation, 1% BSA was added to terminate the labeling reaction. The labeled EVs were incubated with macrophages for 6 h, then free EVs were washed out with PBS. The cells were fixed with 4% paraformaldehyde at room temperature for 20 min. TRITC Phalloidin (Yeasen, Shanghai, China) and 40,6-diamidino-2-phenylindole (DAPI, Sigma-Aldrich) were used to stain the cytoskeleton and nuclei, respectively. Images were captured using an LSM 880 Laser Scanning Confocal Microscope (Zeiss, Jena, Germany).

2.8. RNA Extraction and Real-Time Quantitative PCR. Total RNA from macrophage cells was extracted using TRIzol reagent (Thermo Scientific, MA, U.S.A.). AceQ qPCR SYBR Green Master Mix (Vazyme no. Q111) (Vazyme, China) was utilized in mRNA reverse transcription. Real-time PCR was then conducted with a Phanta Max Master Mix (Vazyme, China). According to the instructions of AceQ qPCR SYBR Green Master Mix, we prepared the reaction solution as follows and performed PCR using a LightCycler480 Instrument II (Roche, Basle, Switzer-land).

- cDNA 1 μL
- SYBR Green Master Mix 10 μL
- Forward Primer (10 μm) 0.8 μL
- Reverse Primer (10 μm) 0.8 μL
- RNase Free Water 7.4 μL

β-actin was used as the internal reference to calculate the relative expression of other genes. The sequence of mRNA primers is described in Text S2:

Relative expression was calculated using the comparative cycle threshold (Ct) method ($2^{-\Delta\Delta CT}$) normalized to β-actin.

2.9. DNA Extraction and Metagenomics Sequencing. EV samples were used to extract DNA following the manufacturer's instructions with the HiPure Soil DNA Kit B (Magen, China). A Qubit 3.0 Fluorometer (Thermo Fisher, Waltham, USA) and agarose gel electrophoresis were used to assess DNA quantity and quality, respectively. The isolated DNAs were stored at −20 °C for later use.

The DNA library construction and sequencing were carried out by the GENEWIZ company (Suzhou, China) using the Illumina platform. For more details on metagenomic sequencing, annotation, and abundance calculation, please refer to the Text S3.

2.10. Raman Spectra Acquisition. Macrophages were dissociated into single cells and fixed in 75% vol/vol ethanol for 1 h. After washing three times with ultrapure water to remove residual media, 3 μL of fixed cells was air-dried on an Al foil at room temperature. The detailed steps for Raman spectra acquisition are provided in Text S4.

2.11. Surprisal Analysis of Raman Spectra. We performed Surprisal analysis (SA) as previously reported[20] which involved analyzing the preprocessed Raman spectra. More details about how the algorithm works can be found in Text S5.

2.12. Protein Preparation and Proteome Analysis. The extraction and quantification of total proteins in EVs were performed by Pierce RIPA buffer (Thermo Scientific, IL, USA)

https://doi.org/10.1021/acs.est.3c04800
Environ. Sci. Technol. XXXX, XXX, XXX−XXX

containing protease inhibitor and Pierce Microplate BCA Protein Assay Kit (Thermo Scientific, IL, USA), respectively.

We employed tandem mass tags (TMT) labeling-based quantitative proteomics to investigate the differential protein expression as previously described.[21,22] For detailed experimental procedures, please refer to Text S6.

2.13. Statistical Analysis. We performed statistical analyses using IBM SPSS 25.0 software (SPSS, Chicago, IL, USA). The data are presented as mean values ± standard deviation (SD). To assess the data differences among multiple groups, we conducted one-way analysis of variance (ANOVA) followed by a post hoc Tukey's test. Statistical significance was considered present with $p < 0.05$.

3. RESULTS AND DISCUSSION

3.1. Pathogens-Derived EVs Carrying VFs Are Abundant in Indoor Dust. Our previous study has confirmed that the microbial EVs were widespread in indoor dust.[19] We further analyzed the profiles of pathogens and VFs-encoding genes in these indoor dust-derived EVs. Metagenomic sequencing predicted that the top five genera of microbial composition were *Pseudomonas* (65.09%), *Aeromonas* (15.09%), *Enterobacter* (5.01%), *Vibrio* (2.28%), and *Bacillus* (1.68%) (Figure 1a). Considering that the *Pseudomonas* genus accounts for only 11.72% in the source dust sample, the relative higher abundance of *Pseudomonas* in EVs showed that it is an efficient producer of EVs released into the environment, implying that these microbes could amply their impact on the host via protruding EVs.[23] These EVs could provide a means of delivering VFs from pathogenic bacteria to the host. We next investigated the VFs-encoding gene profiles of EVs present in the dust sample. 68 VFs including LPS and lipo-oligosaccharides (LOS) were annotated in dust-derived EVs (i.e., VFs and microbial sequences were colocated on the same contigs from EVs samples). These VFs were identified at a high prevalence in EVs. Among the 68 VFs, AdeFGH efflux pump (10.41%), PhoP (8.93%), and AcrAB (7.93%) were the most prevalent (Figure 1b). EVs containing VFs exhibit EVeral benefits, including shielding agents from proteolytic degradation, enhancing concentration and stability, enabling long-range transport, avoiding detection by the immune system, and targeting specific host cells.[24,25] EVs secreted from environmental microbes harbored VFs with high diversity and abundance and thus present a potential threat to human health.

Next, we investigated which host microbes released EVs carrying VFs in dust. EVs carrying VFs were primarily from three dominant genera, *Pseudomonas* (65.75%), *Aeromonas* (14.36%), and *Enterobacter* (5.72%) (Figure 1c). Fifty-three out of the 68 VFs identified were prevalent in Pseudomonas-derived EVs, indicating the diverse range of VFs in these EVs. Thus, *Pseudomonas* could contribute a lot to the potential health hazards caused by indoor dust EVs. Further at the species level, the two main contributors to secrete EVs were *Pseudomonas putidis* (25.12%) and *P. aeruginosa* (22.75%) (Figure 1d). *P. aeruginosa* is one of the most predominant opportunistic pathogens and is responsible for various infections such as bacterial endocarditis, acute pneumonia, and meningitis.[26−28] In light of this, we next investigated the adverse effects of EVs released by the typical model bacterium *P. aeruginosa* PAO1.

It is worth noting that there are some limitations in the current methods for extraction of EVs. Considering that viral particles have sizes similar to that of EVs, the current method for EVs separation cannot exclude the presence of bacteriophages and their possible interference to EVs-macrophage incubation. This requires further investigation.

3.2. Isolation and Characterization of *P. aeruginosa* PAO1-Derived EVs. EVs were collected from the conditioned media of *P. aeruginosa* PAO1 via the differential ultracentrifugation method and characterized by TEM and NanoFCM following the Information for Studies of Extracellular Vesicles 2018 (IEV 2018) guidelines.[29] TEM images showed the presence of a classical "cup-shaped" morphology with a diameter of 50−70 nm (Figure 2a). NanoFCM revealed that most EVs fall

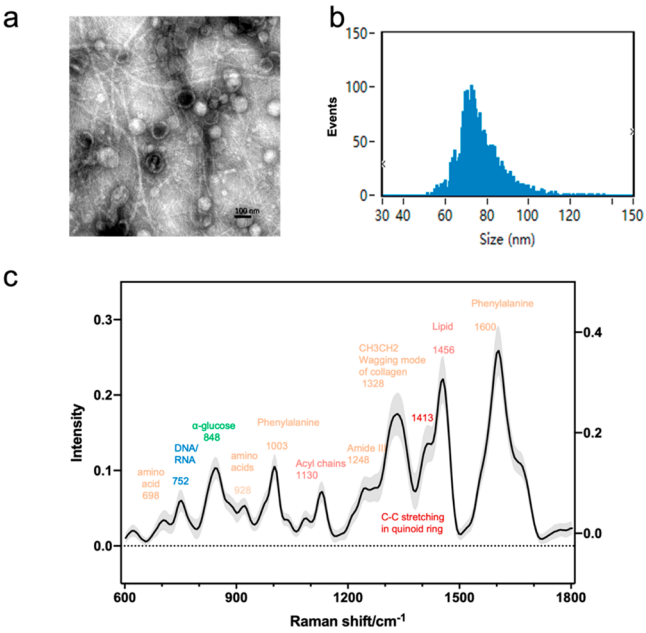

Figure 2. Characterization of EVs released from > *P. aeruginosa* PAO1. (a) Transmission electron microscopy images of EVs from *P. aeruginosa* PAO1, Scale bar = 100 nm. (b) Particle size distribution of *P. aeruginosa* PAO1-derived EVs analyzed by nanoflow cytometer. A range of standard-sized particles (68 to 155 nm) was used as references. (c) Raman spectra of *P. aeruginosa* PAO1-derived EVs. Mean and SD was depicted as the solid line and light shade, respectively. Different colors represent different substance types.

in the size range of 30−150 nm, which is within the typical size ranges of EVs reported in earlier research.[9,30] The average size of *P. aeruginosa* PAO1-derived EVs (PaP-EVs) is 76.6 ± 9.9 nm (Figure 2b). The morphological observation and particle size measurement determined the successful extraction of EVs. By counting a certain number of bacteria and the EVs they produce, we found that each bacterium produced approximately 4.5 EVs (Text S7), highlighting the significant presence of "long-distance weapons" for these pathogens during host infection.

Through the application of Raman spectroscopy, the components of EVs were found to contain various substances including nucleic acids (752 cm^{-1}), proteins (698, 928, 1003, 1248, and 1600 cm^{-1}), carbohydrate (848 and 1456 cm^{-1}), and lipid (1130 and 1328 cm^{-1}) (Figure 2c). The regulation of recipient cells by EVs is primarily achieved through the delivery of their contents, highlighting the potential of bacterial EVs to impact host biological functions.

3.3. *P. aeruginosa* PAO1-Derived EVs Induce Macrophage Inflammatory Response. To investigate the biological effects of EVs on the host, we constructed a coculture model of EVs and macrophages. To be noted, the exposure

https://doi.org/10.1021/acs.est.3c04800
Environ. Sci. Technol. XXXX, XXX, XXX−XXX

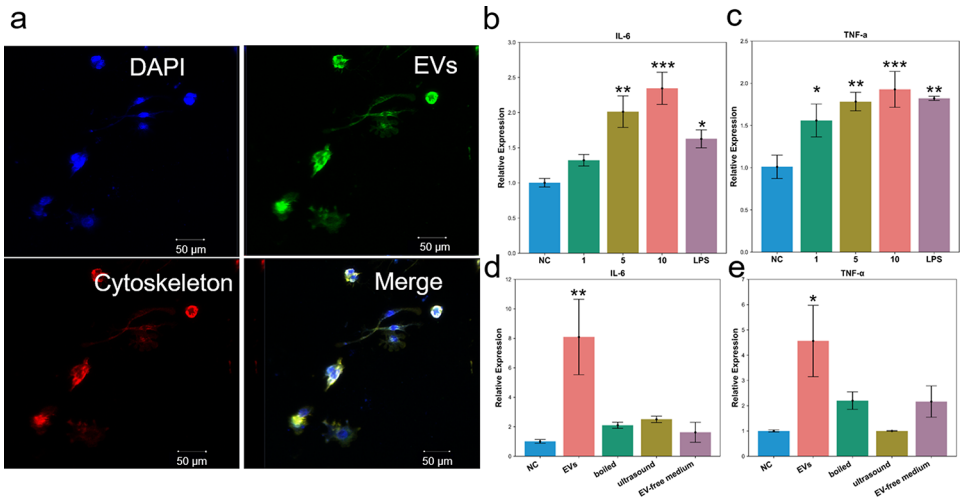

Figure 3. EVs from *P. aeruginosa* PAO1 promoted the expression of inflammatory factors in macrophages. Macrophages were exposed to different concentrations of *P. aeruginosa* PAO1-derived EVs (0, 1, 5, 10 μg/mL) for 24 h. (a) Confocal laser microscopic images of macrophage after exposure to DIO (green)-labeled EVs for 8 h. DAPI (blue) labeled the nuclei, and rhodamine (red) stained the cytoskeleton. Scale bar 50 μm. (b, c) Relative mRNA expressions of IL-6 and TNF-α in macrophages treated with *P. aeruginosa* PAO1-derived EVs. Macrophage exposed to LPS (1 μg/mL) was used as a positive control for the experiment. NC was macrophages exposed to an equal volume of medium without EVs. (d, e) Relative mRNA expressions of IL-6 and TNF-α in macrophage after different treatments including intact EVs, EVs after boiling or ultrasound, EVs-free medium. β-actin was used as an internal control for calibrating the mRNA level. Data are represented as mean ± SD. * represents $p < 0.05$; ** represents $p < 0.01$; *** represents $p < 0.001$.

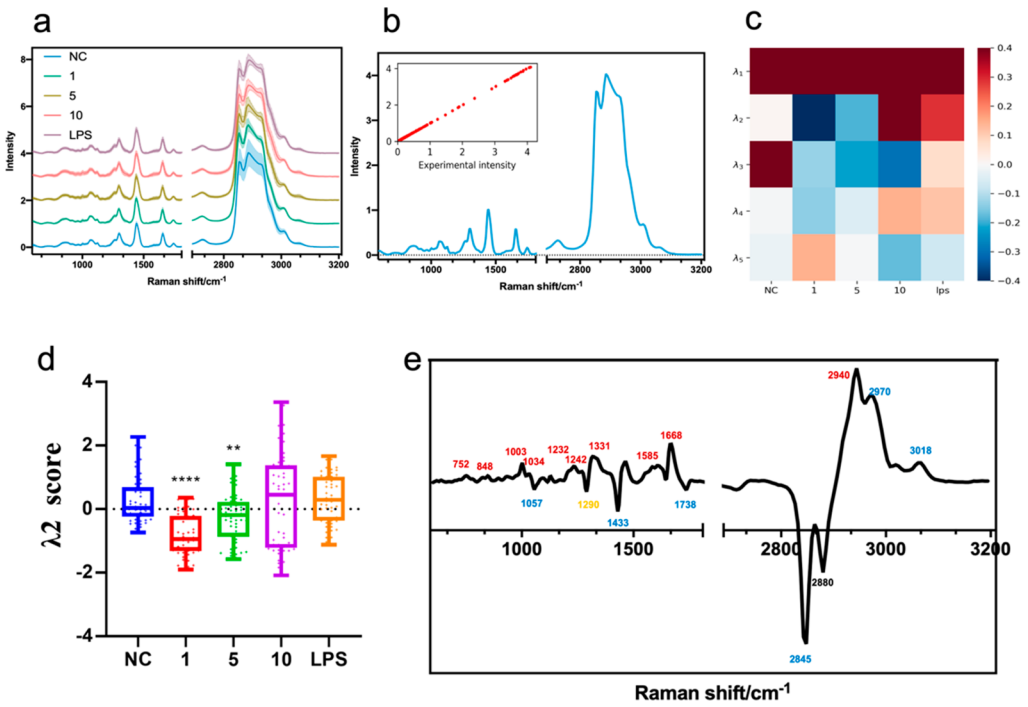

Figure 4. Spontaneous Raman spectra of macrophages exposed to PAO1-derived EVs. (a) Average Raman spectra of macrophage exposed to *P. aeruginosa* PAO1 derived-EV of different concentrations (averaged over 50 cells per treatment group over three independent experiments). The thick solid line and the shadow region represent the mean and standard deviation of the spectra. (b) A typical Raman spectrum of the macrophage was recreated by summing all of the SA disassembled constraints. The inset plot demonstrated the strong correlation between the original and recreated Raman spectrum. (c) Heatmap for the average scores of the top five constraints (λ1-λ5) calculated by SA of the Raman spectra across the five different treatment groups. (d) The variation of λ2 under different treatments. (e) The spectrum of λ2, with Raman peak assignments. Raman peaks labeled red and blue are attributed to proteins and lipids, respectively.

concentrations of EVs were calculated based on the daily exposure doses of a person. However, as there is a the discrepancy between in vitro and in vivo, the dose cannot represent the real doses that macrophages received in lung. We first confirmed that PaP-EVs can enter the macrophages. EVs were labeled with DIO green fluorescent dye. Eight hours after adding EVs to the cell culture media, the green fluorescence was clearly observed within the macrophages, indicating efficient internalization of EVs by macrophages (Figure 3a).

https://doi.org/10.1021/acs.est.3c04800
Environ. Sci. Technol. XXXX, XXX, XXX−XXX

Then, we checked the effects of EVs on macrophages. As *P. aeruginosa* is known to cause inflammatory responses in the host, we evaluated whether PaP-EVs could stimulate the release of inflammatory factors in macrophages. Serial concentrations of PaP-EVs (0, 1, 5, and 10 μg/mL) were incubated with macrophages for 24 h. Meanwhile, LPS which is the main component of Gram-negative bacteria was used as a positive control. Our results showed that exposure to PaP-EVs significantly increased the mRNA level of pro-inflammatory factors IL-6 and TNF-α in macrophages ($p < 0.01$ vs control). RT-PCR quantitative analysis showed that exposure to 1, 5, and 10 μg/mL EVs dose-dependently resulted in respective increases of 31.2%, 100.0%, and 134.2% compared to the IL-6 mRNA levels in the control (Figure 3b). Similarly, the mRNA expression of TNF-α increased by 54.3%, 76.4%, and 90.7% with increasing EV concentrations relative to the control group (Figure 3c). To further confirm the indispensable mediating role of EVs, the vesicle structure was disrupted through boiling and ultrasound before dosing (Figure S1), and the stimulating effects of EVs on the inflammatory factors were almost completely abolished (Figure 3d,e). These results indicate that the mediating roles of complete EVs structure.

3.4. Raman Spectra Distinguish Metabolic Alternations in EVs-Exposed Macrophages. The increased release of inflammatory factors indicated that macrophages may adjust their physiological states to adapt to exposure stress. To better understand the underlying mechanism, macrophages were quickly screened by Raman spectroscopy to explore biochemical changes in response to PaP-EVs exposure (Figure S2). As shown in Figure 4a, it is challenging to distinguish the difference in the spectral range between 600 and 1800 cm^{-1} and 2800−3200 cm^{-1} across macrophages treated with different concentrations of EVs. Hence, an unsupervised Surprisal analysis (SA) algorithm was employed for dimensionality reduction to decipher differences between these spectra.[31] Similar to principal component analysis (PCA), SA decomposed the spectrum into various vectors, which can capture most of the variance in different treated groups.[32] SA has been successfully applied for analyzing gene expression data sets, and it has recently been used to recapitulate fine Raman spectral features.[31] To confirm that this algorithm can indeed capture spectral differences, a series of spectra from 5 pathogenic bacteria with observable variations were used. The spectral differences captured by the SA algorithm were found to be consistent with direct spectral observations, such as the peaks at 1003 and 1584 cm^{-1} (Figure S3), demonstrating its accuracy. Using the SA algorithm, the macrophage spectra were divided into five distinct vectors. We further confirmed that these vectors could accurately reconstruct spectrum shapes with their corresponding weights (Figure 4b and Figure S4). These results indicate that the SA algorithm can capture the subtle differences of spectra between control and PaP-EVs exposed macrophages with high feasibility.

Using the SA model, a heatmap of the top five vectors was generated and labeled as λ1-λ5 in an ascending order, with each group represented by 60 individual cells (Figure 4c,d). λ1 occupies the most interpretation volume, thus capturing most of the common spectral features across different treatment groups. The second vectors, λ2, constituted the secondary interpretation volume and captures most of the variance between spectra. Since the remaining constraints occupy a lower interpretation volume and provide less information regarding spectral features, our analysis of the Raman spectrum primarily relies on the λ2 vector.

The main Raman shifts included in the λ2 vector play an important role in discriminating the metabolic differences of cells under different EVs exposure conditions. The significant Raman shifts in fingerprint region are shown as below: 752 cm^{-1} (symmetric breathing of tryptophan), 848 cm^{-1} (ring breathing of tyrosine),1003 cm^{-1} (ring breathing of phenylalanine), 1034 cm^{-1} (CH in-plane phenylalanine), 1057 cm^{-1} (C−C stretching of lipid), 1232 cm^{-1} (amide III), 1242 cm^{-1} (Amide III), 1290 cm^{-1} (CH_2 bending of cytosine), 1331 cm^{-1} (Collagen), 1433 cm^{-1} (CH_2 bending mode of lipids), 1585 cm^{-1} (C═C bending mode of phenylalanine), 1668 cm^{-1} (Amide I), and 1738 cm^{-1} (C═O stretching of lipids). Most of the observed Raman peaks can be attributed to protein-related substances (Figure 4e), indicating significant changes in the protein content within macrophages during PaP-EVs infection. These alterations in protein peaks may be a result of intracellular responses to pathogen EVs that alter the properties of intracellular enzymes. Additionally, macrophages were demonstrated to release a large quantity of inflammatory factors and cytokines (Figure 3b,c), which are also composed of proteins. This demonstrates that the results of the PCR are consistent with the Raman metabolic phenotype results.

Furthermore, the spectral distribution of λ2 exhibits negative contributions from the lipid peak in the Raman fingerprint region (Figure 4e). This observation suggests opposite changing trend of lipid to that λ2, i.e., that the intensity of these lipid peaks experiences a transition from increase at low exposure concentrations to decrease at high exposure concentrations (Figure S5). The changing trends of lipid may be related to glucose metabolism in macrophages. Glucose serves as the primary energy source for cellular activity. Macrophages exhibited increased carbohydrate and energy consumption to accelerate glycolytic processes and produce precursors for lipid synthesis, such as fatty acids, in response to inflammation.[33] Therefore, the observed increase in lipids at low EVs exposure concentrations may be attributed to inflammation that promoted the glycogenic solution process in macrophages. Conversely, for the decrease in lipids at high EVs exposure concentrations, a plausible reason is that the rapid consumption of energy leads to a switch in the metabolic mode from glycolytic pathways to utilizing lipids as carbon sources. The role of lipid metabolism in macrophage immunity and inflammation has been highlighted in various studies.[34]

The expression of inflammatory factors shows a linear pattern with increasing exposure, which is inconsistent with the Raman results. The reason should be due to the different information that they provided. PCR results indicate changes only in the RNA or genes encoding inflammatory factors. Meanhile Raman spectroscopy and SA results reflect the global biochemical changes in cells including DNA, protein, lipid etc. Although the addition of EVs leads to an elevation of inflammatory genes, they could be only a part of the Raman observation that encompasses not only inflammatory factors but also other biomolecules. Therefore, these two sets of data are not comparable to each other or contradictory.

To further evaluate the alteration of the macrophage lipid during exposure, we analyzed the higher wavenumber region of the Raman spectra between 2800 and 3200 cm^{-1}. Specifically, the lipid peak at 3018 cm^{-1} (unsaturated ═CH stretching of the lipid) and the peak at 2845 cm^{-1} (representing all lipids in the cell) were targeted. The spectral distribution of λ2 shows positive contributions from the 3018 cm^{-1} peak, and negative contributions from the 2845 cm^{-1} peak. Compared to the NC

https://doi.org/10.1021/acs.est.3c04800
Environ. Sci. Technol. XXXX, XXX, XXX−XXX

group, the $\lambda 2$ value of EVs increased at high exposure concentration (10 μg/mL). This indicates that the generated ratio of total unsaturated fatty acids/total fatty acids (TUFA/TFA) revealed an increasing trend from PaP-EVs-exposed macrophages to control groups (Figure 4e). The TUFA/TFA ratio is a commonly used index in Raman studies to characterize lipid membrane profile as an indicator of cell adaptation and response to oxidative stress.[35] Increased lipid unsaturation leads to membrane fluidization and modifications that protect cells against stress. Through rapid screening with Raman spectroscopy, we suggest that macrophage metabolic patterns are greatly altered during EV exposure. Additionally, since the most varied Raman peaks were protein peaks, the proteome was subsequently conducted in an in-depth study.

3.5. *P. aeruginosa* PAO1-Derived EVs Altered the Protein Profile of Macrophage. TMT proteomics was employed to investigate the alternation of the macrophage proteome after exposure. The total protein expression of macrophages exhibited significant differences between exposed groups and the control group (Figure 5a). TMT proteomics

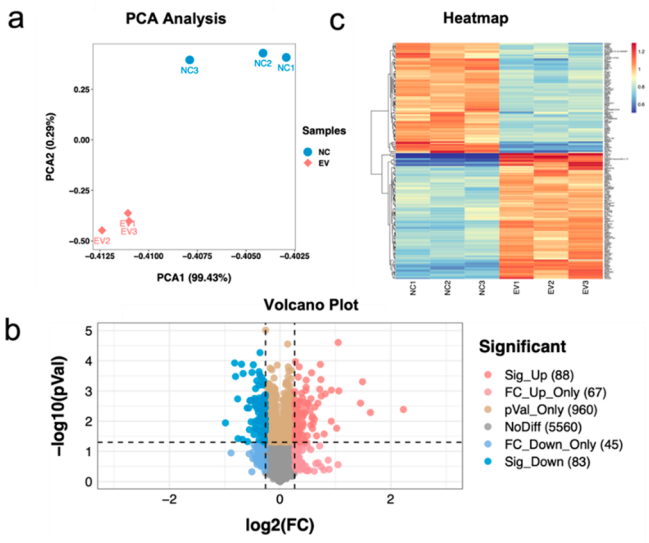

Figure 5. PAO1-derived EVs altered the protein profile of macrophages. (a) PCA analysis showing the pattern of total protein expression in macrophages from the control and EVs exposed group (Adonis, $p = 0.001$). (b) A volcano graphic depicts the total number of detected proteins (6803) and the proteins that were differentially expressed (171). Normalized proteins are regarded as differentially expressed when they have fold changes of >1.2 or <0.83 and a corrected P of 0.05. The peptide identification's false discovery rate (FDR) is estimated to be less than 0.01. (c) Heatmap of the relative expression of differentially expressed proteins in macrophages from control and EVs exposed groups.

identified 6,618 proteins in macrophages. Compared to the control group, 171 differential expressed proteins (DEPs) ($p <$ 0.05, FC > 1.2 or <0.83) were characterized, with 88 up-regulated and 83 down-regulated (Figure 5b,c). GO and KEGG analyses showed that the DEPs were involved in various physiological and pathological processes, such as cellular anatomical entity, cellular process, biological regulation, binding, responses to stimuli, signal transduction, infectious diseases, and the immune system (Figure S6). These suggest that many biological processes of macrophages were significantly altered after exposure to pathogenic EVs.

KEGG enrichment analysis of the DEPs revealed that the up-regulated proteins were enriched in NF-kappa B, cytokine interaction, TNF-α, MAPK, and IL-17 pathways, which are closely related to inflammation and the immune response. This indicates that PaP-EVs activated the inflammation and immune response of macrophages (Figure S7a). Conversely, the down-regulated DEPs were enriched in carbohydrate digestion and absorption, insulin secretion, and other glucose metabolism-related pathways (Figure S7b). The reduced glucose metabolism pathway may be a result of cells conserving energy in an emergency environment. This result supports our Raman phenotype hypothesis that macrophages turned off the glucose metabolic pathway and turned on the lipid metabolic pathways in response to glucose and energy deficiency.

It is noteworthy that although there was no significant enrichment of differential proteins involved in the lipid metabolism, Raman spectroscopy did indicate the affected lipid metabolism. In contrast, the hypothesis generated from Raman spectroscopy data that macrophages were deficient in glucose and energy was subsequently verified by proteomics results. These two methods, Raman spectroscopy and proteomics, complement each other and provide a comprehensive understanding of the metabolic changes that occur in macrophages.

3.6. Metabolic Activity and Inflammatory Response of *P. aeruginosa* PAO1-Derived EVs Exposed Macrophage. Through the enrichment analysis of DEPs, we found that up-regulated DEPs were enriched in inflammatory-related pathways, while down-regulated DEPs were enriched in metabolism-related pathways. Metabolic reprogramming plays an essential role in the inflammatory process.[36] Hence, we used Spearman correlation and co-occurrence network analysis ($p < 0.01$, Pearson's correlation coefficient R > 0.95) to explore the role of metabolic reprogram in the inflammatory response of EVs exposed macrophages. A close correlation was found between inflammatory-related and metabolic-related DEPs, with 63 nodes and 273 edges, indicating that the inflammatory and metabolic responses of macrophages are closely related during the EVs exposure. As demonstrated in Figure S8, metabolism-related DEPs exhibit stronger interactions with DEPs compared to inflammation-related DEPs, suggesting that metabolism-related DEPs play core regulating roles in the network and the activation of the inflammatory response may be governed by the alteration in metabolic regulatory networks under EV exposure. Previous studies have also reported that metabolic reprogramming can play a crucial role in the inflammatory response of macrophages.[37]

3.7. Glucose Starvation Contributes to GFAT and Fuels the HBP Pathway in Macrophage. Modular analysis divided these DEPs in the network map into three modules (Figure S9). The purple module contained more DEPs and exhibited more complexity than other modules. Therefore, DEPs contained in the purple module are considered to be the core protein group in our study. To further elucidate how the reprogrammed cell metabolism process is involved in the inflammatory response of macrophages exposed to PaP-EVs, we analyzed the large nodes (degree > 7) within the core protein group. Consistent with the results obtained from KEGG enrichment analysis, which indicated the activation of inflammation-related pathways, we also observed a significant decrease in the expression of anti-inflammatory factor ASAH1[38,39] and HMOX1[40] (Figure 6a). Other large nodes (degree > 7) were annotated in energy metabolism (ATP1B1, CYP27A1) and glucose metabolism

https://doi.org/10.1021/acs.est.3c04800
Environ. Sci. Technol. XXXX, XXX, XXX−XXX

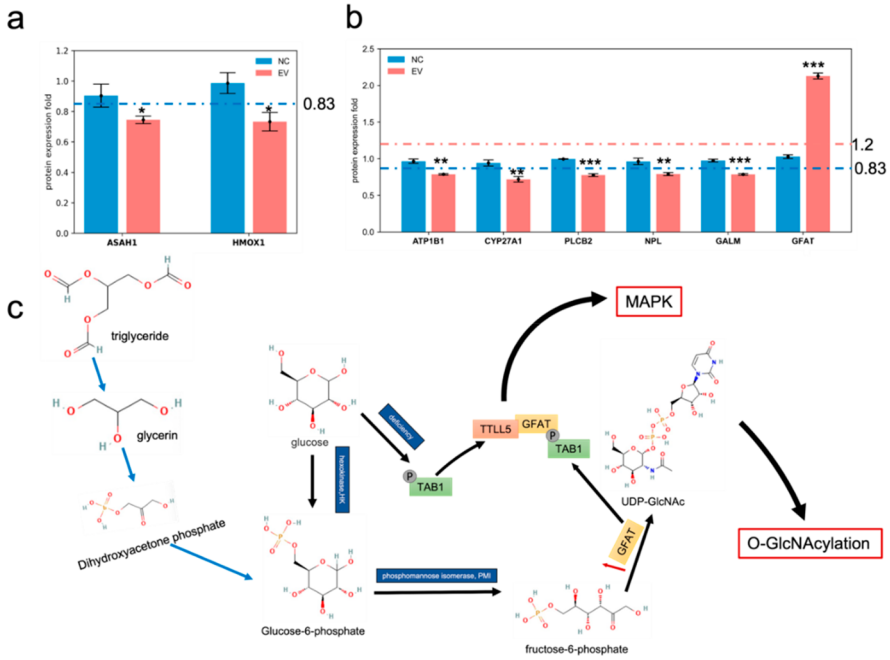

Figure 6. Glucose starvation contributes to GFAT and fuels the HBP pathway in macrophage. (a, b) Relative abundances of anti-inflammatory factors (a) and glycolysis-related proteins based on TMT proteomics. * represents $p < 0.05$; ** represents $p < 0.01$; *** represents $p < 0.001$. (c) A schematic model of the pathway for GFAT-TAB1-MAPK signaling and HBP -the nucleotide sugar UDP-GlcNAc synthesis pathway.

pathways (PLCB2, NPL, GALM, GFAT), with most exhibiting a downregulation trend (Figure 6b). These results are consistent with the findings from Raman spectroscopy and the DEPs enrichment analysis.

Notably, glutamine-fructose-6-phosphate amido transferase 1 (GFAT1), a crucial rate-limiting enzyme in the hexosamine biosynthesis pathway (HBP),[41] was found to be overexpressed with a high expression factor. The HBP pathway constitutes a vital branch of glucose metabolism, acting as a glucose flux sensor that facilitates the regulation of metabolic processes.[42] Earlier studies have demonstrated that during glucose deprivation, GFAT1 is upregulated and the HBP pathway is activated to ensure cellular survival.[43,44] Furthermore, the HBP pathway generates the crucial final product uridine diphosphate-N-acetylglucosamine (UDP-GlcNAc), which serves as a fundamental substrate for protein O-linked β-N-acetylglucosamine (O-GlcNAc) modification (O-GlcNAcylation). O-GlcNAcylation is implicated in gene expression, pathogen infection, and metabolism.[45] Moreover, under glucose-deprived conditions, the metabolic activity of GFAT1 drives glutamylation of TAB1 in a TTLL5-dependent manner, thus activating the MAPK pathway.[46] The combined results of Raman spectroscopy and proteomics analysis demonstrate that under EVs exposure macrophages exhibit a deficiency in glucose, accompanied by a metabolic shift from glucose metabolism to lipid metabolism. This metabolic change activates the HBP pathway, which subsequently triggers O-GlcNAcylation and MAPK pathway activation, further exacerbating the cellular inflammatory response (Figure 6c).

4. ENVIRONMENTAL IMPLICATION

Pathogens in the indoor environment are of great concern for their potential health risk. This work showed that EVs harboring VFs released from Pseudomonas spp. were widely found in indoor dust. These EVs can promote an inflammatory response in macrophages. Mechanistic investigations revealed that macrophages underwent metabolic reprogramming, which can accelerate the inflammatory response. Among them, HBP metabolism and lipid metabolism were identified as important pathways that could potentially serve as regulatory targets in the future. Considering their widespread presence and high stability, diverse VFs carriage, and proinflammatory effects, EVs can be a new mediator for the impact of pathogens on the host in field. The potential health threat posed by environmental pathogen-derived EVs deserves attention from a One-Health perspective.

In addition, we propose a "snapshot" (Raman spectroscopy) combined with a "microscope" (proteomics) approach that enables us to understand the metabolic change by which macrophages respond to environmental EV exposure. Raman spectroscopy acts as a snapshot camera to quickly capture cells' global changes and screen the molecules that undergo the most significant alterations. The sequencing method plays the role of magnifying glass to focus on specific molecules within the most altered cellular composition and to elucidate specific molecular mechanisms. The combination of these two techniques allows for a complementarity and comprehensive analysis of the toxic mechanism. Our method is expected to be applied to investigate the mechanisms of cell response to other environmental pollutants.

■ ASSOCIATED CONTENT

Supporting Information

The Supporting Information is available free of charge at https://pubs.acs.org/doi/10.1021/acs.est.3c04800.

Materials and methods; EVs amounts measurements; laser focal spots on a representative cell; typical pathogens spontaneous Raman spectra analysis; Raman spectrum recreated; changes of lipid peaks; KEGG and GO functional enrichment analyses; network analysis; and modular analysis (PDF)

https://doi.org/10.1021/acs.est.3c04800
Environ. Sci. Technol. XXXX, XXX, XXX−XXX

AUTHOR INFORMATION

Corresponding Authors

Qiansheng Huang − *Xiamen Key Laboratory of Indoor Air and Health, Key Lab of Urban Environment and Health, Institute of Urban Environment, Chinese Academy of Sciences, Xiamen 361021, China;* orcid.org/0000-0002-3788-3164; Phone: 86-592-6190780; Email: qshuang@iue.ac.cn

Li Cui − *Xiamen Key Laboratory of Indoor Air and Health, Key Lab of Urban Environment and Health, Institute of Urban Environment, Chinese Academy of Sciences, Xiamen 361021, China;* orcid.org/0000-0002-0708-8899; Phone: 86-592-6190780; Email: lcui@iue.ac.cn

Authors

Yifei Qin − *Xiamen Key Laboratory of Indoor Air and Health, Key Lab of Urban Environment and Health, Institute of Urban Environment, Chinese Academy of Sciences, Xiamen 361021, China; College of Resources and Environment, University of Chinese Academy of Sciences, Beijing 100049, China*

Zheng Shi − *College of Resources and Environment, University of Chinese Academy of Sciences, Beijing 100049, China; State Environment Protection Key Laboratory of Satellite Remote Sensing, Aerospace Information Research Institute, Chinese Academy of Sciences, Beijing 100101, China*

Longji Zhu − *Xiamen Key Laboratory of Indoor Air and Health, Key Lab of Urban Environment and Health, Institute of Urban Environment, Chinese Academy of Sciences, Xiamen 361021, China*

Hongzhe Li − *Xiamen Key Laboratory of Indoor Air and Health, Key Lab of Urban Environment and Health, Institute of Urban Environment, Chinese Academy of Sciences, Xiamen 361021, China*

Wenjia Lu − *Xiamen Key Laboratory of Indoor Air and Health, Key Lab of Urban Environment and Health, Institute of Urban Environment, Chinese Academy of Sciences, Xiamen 361021, China; College of Resources and Environment, University of Chinese Academy of Sciences, Beijing 100049, China*

Guozhu Ye − *Xiamen Key Laboratory of Indoor Air and Health, Key Lab of Urban Environment and Health, Institute of Urban Environment, Chinese Academy of Sciences, Xiamen 361021, China;* orcid.org/0000-0001-5173-2293

Complete contact information is available at: https://pubs.acs.org/10.1021/acs.est.3c04800

Author Contributions

Y.F.Q., Q.S.H., and L.C. prepared the manuscript and conducted data analysis. L.J.Z. and W.J.L. contributed to sample collecting. Y.F.Q. and Z.H.L. performed the experiment. G.Z.Y. and Z.S. helped perform the analysis with constructive discussions. All coauthors provided intellectual and substantive contributions to the manuscript.

Notes

The authors declare no competing financial interest.

ACKNOWLEDGMENTS

This work was supported by National Natural Science Foundation of China (NSFC) (22176186), Chinese Academy of Sciences (ZDBS-LY-DQC027), NSFC (32161143016, 42177362, 42250410328), and Fujian Provincial Department of Science and Technology (2022T3063).

REFERENCES

(1) Klepeis, N. E.; Nelson, W.C.; Ott, W.R.; Robinson, J.P.; Tsang, A.M.; Switzer, P.; Behar, J.V.; Hern, S.C.; Engelmann, W.H. The National Human Activity Pattern Survey (Nhaps): A Resource for Assessing Exposure to Environmental Pollutantrs. *J. Expo Anal Environ. Epidemiol* **2001**, *11* (3), 231−252.

(2) Cincinelli, A.; Martellini, T. Indoor Air Quality and Health. *Int. J. Environ. Res. Public Health* **2017**, *14* (11), 1286.

(3) Zhu, D.; Zhang, Y.; Zhu, Y.-G. Human Pathogens in the Soil Ecosystem: Occurrence, Dispersal, and Study Method. *Current Opinion in Environmental Science & Health* **2023**, *33*, 100471.

(4) Shao, H.; Im, H.; Castro, C.M.; Breakefield, X.; Weissleder, R.; Lee, H. New Technologies for Analysis of Extracellular Vesicles. *Chem. Rev.* **2018**, *118* (4), 1917−1950.

(5) Toyofuku, M.; Nomura, N.; Eberl, L. Types and Origins of Bacterial Membrane Vesicles. *Nat. Rev. Microbiol* **2019**, *17* (1), 13−24.

(6) Colombo, M.; Raposo, G.; Thery, C. Biogenesis, Secretion, and Intercellular Interactions of Exosomes and Other Extracellular Vesicles. *Annu. Rev. Cell Dev Biol.* **2014**, *30*, 255−289.

(7) EL Andaloussi, S.; Mäger, I.; Breakefield, X. O.; Wood, M. J. A. Extracellular Vesicles: Biology and Emerging Therapeutic Opportunities. *Nat. Rev. Drug Discov* **2013**, *12* (5), 347−37.

(8) Kaparakis-Liaskos, M.; Ferrero, R.L. Immune Modulation by Bacterial Outer Membrane Vesicles. *Nat. Rev. Immunol* **2015**, *15* (6), 375−387.

(9) Schwechheimer, C.; Kuehn, M.J. Outer-Membrane Vesicles from Gram-Negative Bacteria: Biogenesis and Functions. *Nat. Rev. Microbiol* **2015**, *13* (10), 605−619.

(10) Bittel, M.; Reichert, P.; Sarfati, I.; Dressel, A.; Leikam, S.; Uderhardt, S.; Stolzer, I.; Phu, T.A.; Ng, M.; Vu, N.K.; Tenzer, S.; Distler, U.; Wirtz, S.; Rothhammer, V.; Neurath, M.F.; Raffai, R.L.; Gunther, C.; Momma, S. Visualizing Transfer of Microbial Biomolecules by Outer Membrane Vesicles in Microbe-Host-Communication in Vivo. *Journal of Extracellular Vesicles* **2021**, *10* (12), e12159.

(11) Armstrong, D. A.; Lee, M.K.; Hazlett, H.F.; Dessaint, J.A.; Mellinger, D.L.; Aridgides, D.S.; Hendricks, G.M.; Abdalla, M. A. K.; Christensen, B.C.; Ashare, A. Extracellular Vesicles from Pseudomonas Aeruginosa Suppress Mhc-Related Molecules in Human Lung Macrophages. *Immunohorizons* **2020**, *4* (8), 508−519.

(12) Deo, P.; Chow, S.H.; Han, M.L.; Speir, M.; Huang, C.; Schittenhelm, R.B.; Dhital, S.; Emery, J.; Li, J.; Kile, B.T.; Vince, J.E.; Lawlor, K.E.; Naderer, T. Mitochondrial Dysfunction Caused by Outer Membrane Vesicles from Gram-Negative Bacteria Activates Intrinsic Apoptosis and Inflammation. *Nat. Microbiol* **2020**, *5* (11), 1418−1427.

(13) Dinh, N. T. H.; Lee, J.; Lee, J.; Kim, S.S.; Go, G.; Bae, S.; Jun, Y.I.; Yoon, Y.J.; Roh, T.Y.; Gho, Y.S. Indoor Dust Extracellular Vesicles Promote Cancer Lung Metastasis by Inducing Tumour Necrosis Factor-Alpha. *J. Extracell Vesicles* **2020**, *9* (1), 1766821.

(14) Keller, M. A.; Piedrafita, G.; Ralser, M. The Widespread Role of Non-Enzymatic Reactions in Cellular Metabolism. *Curr. Opin Biotechnol* **2015**, *34*, 153−161.

(15) Lima, C.; Muhamadali, H.; Goodacre, R. The Role of Raman Spectroscopy within Quantitative Metabolomics. *Annu. Rev. Anal Chem. (Palo Alto Calif)* **2021**, *14* (1), 323−345.

(16) Zong, C.; Xu, M.; Xu, L.J.; Wei, T.; Ma, X.; Zheng, X.S.; Hu, R.; Ren, B. Surface-Enhanced Raman Spectroscopy for Bioanalysis: Reliability and Challenges. *Chem. Rev.* **2018**, *118* (10), 4946−4980.

(17) Butler, H. J.; Ashton, L.; Bird, B.; Cinque, G.; Curtis, K.; Dorney, J.; Esmonde-White, K.; Fullwood, N.J.; Gardner, B.; Martin-Hirsch, P. L.; Walsh, M.J.; McAinsh, M.R.; Stone, N.; Martin, F.L. Using Raman Spectroscopy to Characterize Biological Materials. *Nat. Protoc* **2016**, *11* (4), 664−87.

(18) Qin, Y.; Guo, Z.; Huang, H.; Zhu, L.; Dong, S.; Zhu, Y.G.; Cui, L.; Huang, Q. Widespread of Potential Pathogen-Derived Extracellular Vesicles Carrying Antibiotic Resistance Genes in Indoor Dust. *Environ. Sci. Technol.* **2022**, *56* (9), 5653−5663.

https://doi.org/10.1021/acs.est.3c04800
Environ. Sci. Technol. XXXX, XXX, XXX−XXX

(19) U.S. EPA *Exposure Factors Handbook 2011 Edition*, 2021. https://cfpub.epa.gov/ncea/risk/recordisplay.cfm?deid=236252 [accessed 2023 18th June].
(20) Ozkaynak, H.; Xue, J.; Zartarian, V.G.; Glen, G.; Smith, L. Modeled Estimates of Soil and Dust Ingestion Rates for Children. *Risk Anal* **2011**, *31* (4), 592−608.
(21) Lyu, K.; Meng, Q.; Zhu, X.; Dai, D.; Zhang, L.; Huang, Y.; Yang, Z. Changes in Itraq-Based Proteomic Profiling of the Cladoceran Daphnia Magna Exposed to Microcystin-Producing and Microcystin-Free Microcystis Aeruginosa. *Environ. Sci. Technol.* **2016**, *50* (9), 4798−4807.
(22) Wan, R.; Chen, Y.; Zheng, X.; Su, Y.; Li, M. Effect of Co2 on Microbial Denitrification Via Inhibiting Electron Transport and Consumption. *Environ. Sci. Technol.* **2016**, *50* (18), 9915−9922.
(23) Zhu, L. T.; Huang, H. N.; Avellan-Llaguno, R. D.; Qin, Y.; An, X. L.; Su, J.Q.; Huang, Q.; Zhu, Y.G. Diverse Functional Genes Harboured in Extracellular Vesicles from Environmental and Human Microbiota. *J. Extracell Vesicles* **2022**, *11* (12), 12292.
(24) Bonnington, K. E.; Kuehn, M.J. Protein Selection and Export Via Outer Membrane Vesicles. *Biochim. Biophys. Acta* **2014**, *1843* (8), 1612−1619.
(25) Cecil, J. D.; Sirisaengtaksin, N.; O'Brien-Simpson, N. M.; Krachler, A.M. Outer Membrane Vesicle-Host Cell Interactions. *Microbiol Spectr* **2019**, DOI: 10.1128/microbiolspec.PSIB-0001-2018.
(26) Gellatly, S. L.; Handock, R.E. Pseudomonas Aeruginosa: New Insights into Pathogenesis and Host Defenses. *Pathog Dis* **2013**, *67* (3), 159−173.
(27) Nathwani, D.; Raman, G.; Sulham, K.; Gavaghan, M.; Menon, V. Clinical and Economic Consequences of Hospital-Acquired Resistant and Multidrug-Resistant Pseudomonas Aeruginosa Infections: A Systematic Review and Meta-Analysis. *Antimicrob Resist Infect Control* **2014**, *3* (1), 32.
(28) Weiner, L. M.; Webb, A.K.; Limbago, B.; Dudeck, M.A.; Patel, J.; Kallen, A.J.; Edwards, J.R.; Sievert, D.M. Antimicrobial-Resistant Pathogens Associated with Healthcare-Associated Infections: Summary of Data Reported to the National Healthcare Safety Network at the Centers for Disease Control and Prevention, 2011−2014. *Infect Control Hosp Epidemiol* **2016**, *37* (11), 1288−1301.
(29) Théry, C.; Witwer, K. W.; Aikawa, E.; Alcaraz, M. J.; Anderson, J. D.; Andriantsitohaina, R.; Antoniou, A.; Arab, T.; Archer, F.; Atkin-Smith, G. K; Ayre, D. C.; Bach, J.-M.; Bachurski, D.; Baharvand, H.; Balaj, L.; Baldacchino, S.; Bauer, N. N.; Baxter, A. A; Bebawy, M.; Beckham, C.; Bedina Zavec, A.; Benmoussa, A.; Berardi, A. C.; Bergese, P.; Bielska, E.; Blenkiron, C.; Bobis-Wozowicz, S.; Boilard, E.; Boireau, W.; Bongiovanni, A.; Borràs, F. E.; Bosch, S.; Boulanger, C. M.; Breakefield, X.; Breglio, A. M.; Brennan, M. A.; Brigstock, D. R.; Brisson, A.; Broekman, M. L.; Bromberg, J. F.; Bryl-Gorecka, P.; Buch, S.; Buck, A. H.; Burger, D.; Busatto, S.; Buschmann, D.; Bussolati, B.; Buzás, E. I; Byrd, J. B.; Camussi, G.; Carter, D. R.; Caruso, S.; Chamley, L. W.; Chang, Y.-T.; Chen, C.; Chen, S.; Cheng, L.; Chin, A. R.; Clayton, A.; Clerici, S. P.; Cocks, A.; Cocucci, E.; Coffey, R. J.; Cordeiro-da-Silva, A.; Couch, Y.; Coumans, F. A.; Coyle, B.; Crescitelli, R.; Criado, M. F.; DSouza-Schorey, C.; Das, S.; Datta Chaudhuri, A.; de Candia, P.; E. F., De Santana; De Wever, O.; del Portillo, H. A.; Demaret, T.; Deville, S.; Devitt, A.; Dhondt, B.; Di Vizio, D.; Dieterich, L. C.; Dolo, V.; Dominguez Rubio, A. P.; Dominici, M.; Dourado, M. R.; Driedonks, T. A.; Duarte, F. V.; Duncan, H. M.; Eichenberger, R. M.; Ekstrom, K.; EL Andaloussi, S.; Elie-Caille, C.; Erdbrugger, U.; Falcón-Pérez, J. M.; Fatima, F.; Fish, J. E.; Flores-Bellver, M.; Försönits, A.; Frelet-Barrand, A.; Fricke, F.; Fuhrmann, G.; Gabrielsson, S.; Gámez-Valero, A.; Gardiner, C.; Gärtner, K.; Gaudin, R.; Gho, Y. S.; Giebel, B.; Gilbert, C.; Gimona, M.; Giusti, I.; Goberdhan, D. C.; Görgens, A.; Gorski, S. M.; Greening, D. W.; Gross, J. C.; Gualerzi, A.; Gupta, G. N.; Gustafson, D.; Handberg, A.; Haraszti, R. A.; Harrison, P.; Hegyesi, H.; Hendrix, A.; Hill, A. F.; Hochberg, F. H.; Hoffmann, K. F.; Holder, B.; Holthofer, H.; Hosseinkhani, B.; Hu, G.; Huang, Y.; Huber, V.; Hunt, S.; Ibrahim, A. G.-E.; Ikezu, T.; Inal, J. M.; Isin, M.; Ivanova, A.; Jackson, H. K.; Jacobsen, S.; Jay, S. M.; Jayachandran, M.; Jenster, G.; Jiang, L.; Johnson, S. M.; Jones, J. C.; Jong, A.; Jovanovic-Talisman, T.; Jung, S.; Kalluri, R.; Kano, S.-i.; Kaur, S.; Kawamura, Y.; Keller, E. T.; Khamari, D.; Khomyakova, E.; Khvorova, A.; Kierulf, P.; Kim, K. P.; Kislinger, T.; Klingeborn, M.; Klinke, D. J.; Kornek, M.; Kosanović, M. M.; Kovács, Á. F.; Kramer-Albers, E.-M.; Krasemann, S.; Krause, M.; Kurochkin, I. V.; Kusuma, G. D.; Kuypers, S.; Laitinen, S.; Langevin, S. M.; Languino, L. R; Lannigan, J.; Lässer, C.; Laurent, L. C.; Lavieu, G.; Lázaro-Ibáñez, E.; Le Lay, S.; Lee, M.-S.; Lee, Y. X. F.; Lemos, D. S.; Lenassi, M.; Leszczynska, A.; Li, I. T.; Liao, K.; Libregts, S. F.; Ligeti, E.; Lim, R.; Lim, S. K.; Linē, A.; Linnemannstons, K.; Llorente, A.; Lombard, C. A.; Lorenowicz, M. J.; Lörincz, A. M.; Lötvall, J.; Lovett, J.; Lowry, M. C; Loyer, X.; Lu, Q.; Lukomska, B.; Lunavat, T. R.; Maas, S. L.; Malhi, H.; Marcilla, A.; Mariani, J.; Mariscal, J.; Martens-Uzunova, E. S.; Martin-Jaular, L.; Martinez, M. C.; Martins, V. R.; Mathieu, M.; Mathivanan, S.; Maugeri, M.; McGinnis, L. K.; McVey, M. J.; Meckes, D. G.; Meehan, K. L; Mertens, I.; Minciacchi, V. R.; Möller, A.; Møller Jørgensen, M.; Morales-Kastresana, A.; Morhayim, J.; Mullier, F.; Muraca, M.; Musante, L.; Mussack, V.; Muth, D. C.; Myburgh, K. H.; Najrana, T.; Nawaz, M.; Nazarenko, I.; Nejsum, P.; Neri, C.; Neri, T.; Nieuwland, R.; Nimrichter, L.; Nolan, J. P.; Noltet Hoen, E. N.; Noren Hooten, N.; O'Driscoll, L.; O'Grady, T.; O'Loghlen, A.; Ochiya, T.; Olivier, M.; Ortiz, A.; Ortiz, L. A.; Osteikoetxea, X.; Østergaard, O.; Ostrowski, M.; Park, J.; Pegtel, D. M.; Peinado, H.; Perut, F.; Pfaffl, M. W.; Phinney, D. G.; Pieters, B. C.; Pink, R. C.; Pisetsky, D. S.; Pogge von Strandmann, E.; Polakovicova, I.; Poon, I. K.; Powell, B. H.; Prada, I.; Pulliam, L.; Quesenberry, P.; Radeghieri, A.; Raffai, R. L.; Raimondo, S.; Rak, J.; Ramirez, M. I.; Raposo, G.; Rayyan, M. S.; Regev-Rudzki, N.; Ricklefs, F. L.; Robbins, P. D.; Roberts, D. D.; Rodrigues, S. C.; Rohde, E.; Rome, S.; Rouschop, K. M.; Rughetti, A.; Russell, A. E.; Saá, P.; Sahoo, S.; Salas-Huenuleo, E.; Sanchez, C.; Saugstad, J. A.; Saul, M. J.; Schiffelers, R. M.; Schneider, R.; Schøyen, T. H.; Scott, A.; Shahaj, E.; Sharma, S.; Shatnyeva, O.; Shekari, F.; Shelke, G. V.; Shetty, A. K.; Shiba, K.; Siljander, P. R.-M.; Silva, A. M.; Skowronek, A.; Snyder, O. L.; Soares, R. P.; Sodar, B. W.; Soekmadji, C.; Sotillo, J.; Stahl, P. D.; Stoorvogel, W.; Stott, S. L.; Strasser, E. F.; Swift, S.; Tahara, H.; Tewari, M.; Timms, K.; Tiwari, S.; Tixeira, R.; Tkach, M.; Toh, W. S.; Tomasini, R.; Torrecilhas, A. C.; Tosar, J. P.; Toxavidis, V.; Urbanelli, L.; Vader, P.; van Balkom, B. W.; van der Grein, S. G.; Van Deun, J.; van Herwijnen, M. J.; Van Keuren-Jensen, K.; van Niel, G.; van Royen, M. E.; van Wijnen, A. J.; Vasconcelos, M. H.; Vechetti, I. J.; Veit, T. D.; Vella, L. J.; Velot, E.; Verweij, F. J.; Vestad, B.; Viñas, J. L.; Visnovitz, T.; Vukman, K. V.; Wahlgren, J.; Watson, D. C.; Wauben, M. H.; Weaver, A.; Webber, J. P.; Weber, V.; Wehman, A. M.; Weiss, D. J.; Welsh, J. A.; Wendt, S.; Wheelock, A. M.; Wiener, Z.; Witte, L.; Wolfram, J.; Xagorari, A.; Xander, P.; Xu, J.; Yan, X.; Yáñez-Mó, M.; Yin, H.; Yuana, Y.; Zappulli, V.; Zarubova, J.; Zekas, V.; Zhang, J.-y.; Zhao, Z.; Zheng, L.; Zheutlin, A. R.; Zickler, A. M.; Zimmermann, P.; Zivkovic, A. M.; Zocco, D.; Zuba-Surma, E. K. Minimal Information for Studies of Extracellular Vesicles 2018 (Misev2018): A Position Statement of the International Society for Extracellular Vesicles and Update of the Misev2014 Guidelines *J. Extracell Vesicles* **2018**, *7* (1) 1535750.
(30) Brown, L.; Wolf, J.M.; Prados-Rosales, R.; Casadevall, A. Through the Wall: Extracellular Vesicles in Gram-Positive Bacteria, Mycobacteria and Fungi. *Nat. Rev. Microbiol* **2015**, *13* (10), 620−30.
(31) Du, J.; Su, Y.; Qian, C.; Yuan, D.; Miao, K.; Lee, D.; Ng, A. H. C.; Wijker, R.S.; Ribas, A.; Levine, R.D.; Heath, J.R.; Wei, L. Raman-Guided Subcellular Pharmaco-Metabolomics for Metastatic Melanoma Cells. *Nat. Commun.* **2020**, *11* (1), 4830.
(32) Remacle, F.; Kravchenko-Balasha, N.; Levitzki, A.; Levine, R.D. Information-Theoretic Analysis of Phenotype Changes in Early Stages of Carcinogenesis. *Proc. Natl. Acad. Sci. U. S. A.* **2010**, *107* (22), 10324−10329.
(33) Jha, A. K.; Huang, S.C.; Sergushichev, A.; Lampropoulou, V.; Ivanova, Y.; Loginicheva, E.; Chmielewski, K.; Stewart, K.M.; Ashall, J.; Everts, B.; Pearce, E.J.; Driggers, E.M.; Artyomov, M.N. Network Integration of Parallel Metabolic and Transcriptional Data Reveals Metabolic Modules That Regulate Macrophage Polarization. *Immunity* **2015**, *42* (3), 419−30.

https://doi.org/10.1021/acs.est.3c04800
Environ. Sci. Technol. XXXX, XXX, XXX−XXX

(34) Yan, J.; Horng, T. Lipid Metabolism in Regulation of Macrophage Functions. *Trends Cell Biol.* **2020**, *30* (12), 979−989.
(35) Potcoava, M. C.; Futia, G.L.; Aughenbaugh, J.; Schlaepfer, I.R.; Gibson, E.A. Raman and Coherent Anti-Stokes Raman Scattering Microscopy Studies of Changes in Lipid Content and Composition in Hormone-Treated Breast and Prostate Cancer Cells. *J. Biomed Opt* **2014**, *19* (11), 111605.
(36) Mak, T. W.; Grusdat, M.; Duncan, G.S.; Dostert, C.; Nonnenmacher, Y.; Cox, M.; Binsfeld, C.; Hao, Z.; Brustle, A.; Itsumi, M.; Jager, C.; Chen, Y.; Pinkenburg, O.; Camara, B.; Ollert, M.; Bindslev-Jensen, C.; Vasiliou, V.; Gorrini, C.; Lang, P.A.; Lohoff, M.; Harris, I.S.; Hiller, K.; Brenner, D. Glutathione Primes T Cell Metabolism for Inflammation. *Immunity* **2017**, *46* (4), 675−689.
(37) Kelly, B.; O'Neill, L. A. Metabolic Reprogramming in Macrophages and Dendritic Cells in Innate Immunity. *Cell Res.* **2015**, *25* (7), 771−784.
(38) Jiang, Y.; He, X.; Simonaro, C.M.; Yi, B.; Schuchman, E.H. Acid Ceramidase Protects against Hepatic Ischemia/Reperfusion Injury by Modulating Sphingolipid Metabolism and Reducing Inflammation and Oxidative Stress. *Front Cell Dev Biol.* **2021**, *9*, 633657.
(39) Simoes, M.; Saleh, A.; Choi, Y.M.; Airola, M.V.; Haley, J.D.; Coant, N. Measurement of Neutral Ceramidase Activity in Vitro and in Vivo. *Anal. Biochem.* **2022**, *643*, 114577.
(40) Deng, X.; Liang, C.; Qian, L.; Zhang, Q. Mir-24 Targets Hmox1 to Regulate Inflammation and Neurofunction in Rats with Cerebral Vasospasm after Subarachnoid Hemorrhage. *Am. J. Transl Res.* **2021**, *13* (3), 1064−1074.
(41) Shi, Q.; Shen, Q.; Liu, Y.; Shi, Y.; Huang, W.; Wang, X.; Li, Z.; Chai, Y.; Wang, H.; Hu, X.; Li, N.; Zhang, Q.; Cao, X. Increased Glucose Metabolism in Tams Fuels O-Glcnacylation of Lysosomal Cathepsin B to Promote Cancer Metastasis and Chemoresistance. *Cancer Cell* **2022**, *40* (10), 1207−1222.
(42) Wei, S. P.; Zhao, Q.; Zheng, K.; Liu, P.Y.; Sha, N.N.; Li, Y.Z.; Ma, C.M.; Li, J.J.; Zhuo, L.G.; Liu, G.X.; Liang, W.H.; Jiang, Y.H.; Chen, T.; Zhong, N.S. Gfat1-Linked Tab1 Glutamylation Sustains P38 Mapk Activation and Promotes Lung Cancer Cell Survival under Glucose Starvation. *Cell Discovery* **2022**, *8* (1), 77.
(43) Moloughney, J. G.; Kim, P. K.; Vega-Cotto, N. M.; Wu, C. C.; Zhang, S.; Adlam, M.; Lynch, T.; Chou, P. C.; Rabinowitz, J. D.; Werlen, G.; Jacinto, E. Mtorc2 Responds to Glutamine Catabolite Levels to Modulate the Hexosamine Biosynthesis Enzyme Gfat1. *Mol. Cell* **2016**, *63* (5), 811−826.
(44) Moloughney, J. G.; Vega-Cotto, N. M.; Liu, S.; Patel, C.; Kim, P.K.; Wu, C.C.; Albaciete, D.; Magaway, C.; Chang, A.; Rajput, S.; Su, X.; Werlen, G.; Jacinto, E. Mtorc2Modulates the Amplitude and Duration of Gfat1 Ser-243 Phosphorylation to Maintain Flux through the Hexosamine Pathway During Starvation. *J. Biol. Chem.* **2018**, *293* (42), 16464−16478.
(45) Hwang, J. S.; Kim, K.H.; Park, J.; Kim, S.M.; Cho, H.; Lee, Y.; Han, I.O. Glucosamine Improves Survival in a Mouse Model of Sepsis and Attenuates Sepsis-Induced Lung Injury and Inflammation. *J. Biol. Chem.* **2019**, *294* (2), 608−622.
(46) Wei, S.; Zhao, Q.; Zheng, K.; Liu, P.; Sha, N.; Li, Y.; Ma, C.; Li, J.; Zhuo, L.; Liu, G.; Liang, W.; Jiang, Y.; Chen, T.; Zhong, N. Gfat1-Linked Tab1 Glutamylation Sustains P38 Mapk Activation and Promotes Lung Cancer Cell Survival under Glucose Starvation. *Cell Discov* **2022**, *8* (1), 77.

https://doi.org/10.1021/acs.est.3c04800
Environ. Sci. Technol. XXXX, XXX, XXX−XXX